Available online at www.sciencedirect.com
SCIENCE DIRECT®
International Journal of Heat and Mass Transfer 47 (2004) 4469–4478
International Journal of HEAT and MASS TRANSFER
www.elsevier.com/locate/ijhmt

Spreading and solidification of a molten metal droplet impinging on a heated surface

D. Sivakumar *, H. Nishiyama

Electromagnetic Intelligent Fluids Laboratory, Institute of Fluid Science, Tohoku University, 2-1-1, Katahira, Aoba-ku, Sendai 980-8577, Japan

Received 2 October 2003
Available online 3 July 2004

Abstract

The spreading and solidification processes of a molten metal droplet impinging on a heated solid surface are studied theoretically. The present work is based on Madejski's splat-quench solidification model proposed for the application of plasma spray coating. In contrast to the original model, the initial conditions are modeled in the present work at an instant away from the start of impact. The numerical results on the evolution of the droplet spreading obtained from the present model are compared with the predictions of previous model and available experimental data reported in the literature. It is shown that the present model predictions are in good agreement with the experimental measurements for the inertia driven droplet impact cases. It is further shown that the present model is more suitable for the droplet impact cases showing low Stefan number and high Peclet number.

1. Introduction

Modeling the impact process of a molten metal droplet impinging on a flat surface is received considerable attention in recent years due to its importance in several advanced technologies [1–5]. The problem involves an analysis of the radial spreading of molten metal liquid, caused mainly by the inertia of the impinging droplet, along with the heat transfer and solidification processes occurring simultaneously. Several theoretical studies have been carried out over years to predict the outcomes of the impact process. Zhao et al. [6,7] and Pasandideh-Fard et al. [8] proposed detail models by solving the Navier–Stokes equation coupled with the energy equation. Their theoretical predictions of the droplet spreading were in good agreement with the experimental data. However, the numerical procedures adopted in those models were computationally expensive. Such detailed models are more useful to get a deep fundamental understanding on the physical processes involved in the impact phenomenon. On the other hand, many researchers proposed simple analytical solutions to estimate the outcomes of droplet impact, for example the maximum spread radius, R_{max} and thickness, b_{max} of the metal splat resulting from the impact [9–15]. Evidently, these results are of limited use due to the assumptions involved in the analysis.

Madejski [10] proposed a simple model for the impact of molten metal droplets based on the principle of energy conservation. The model can be used to predict the temporal evolution of the spreading droplet radius, R, however no attempt was made by Madejski to solve the governing equations numerically. Delplanque and Rangel [13] incorporated major modifications into the Madejski's original model [10] and solved the governing differential equation numerically to obtain the temporal variation of R and other relevant parameters. The improved model [13], hereafter referred in this paper as *DR model*, retained the original assumptions and salient features of the Madejski's model [10] and corrections were given for the flow field description and viscous dissipation losses [13]. A detailed parametric study was carried out without making any comparison of the model predictions with the experimental results [13].

* Corresponding author. Tel./fax: +81-22-217-5261.
E-mail address: siva@paris.ifs.tohoku.ac.jp (D. Sivakumar).

0017-9310/$ - see front matter © 2004 Elsevier Ltd. All rights reserved.
doi:10.1016/j.ijheatmasstransfer.2004.02.030

Nomenclature

b	liquid layer thickness of spreading droplet
$\bar{b}_0$	the ratio of liquid layer thickness of spreading droplet in the absence of solidification to droplet diameter before impact
C	time dependent quantity shown in velocity field
C_p	specific heat
Ca	capillary number
D	droplet diameter before impact
E_d	dissipation energy
E_k	kinetic energy
E_p	potential energy
h_f	latent heat of fusion
K	solidification parameter
Oh	Ohnesorge number
Pe	Peclet number
R	radius of spreading droplet
Re	Reynolds number
r	radial coordinate
St	Stefan number
T_0	substrate temperature
T_m	melting temperature of droplet material
t	time
$\tilde{t}$	non-dimensionalized time
t^*	dimensionless time based on impinging droplet parameters
U	solidification constant
V_s	volume of solidified metal layer
W	droplet impact velocity
W_c	liquid contact line velocity
We	Weber number
y	thickness of solidified metal layer
z	normal coordinate

Greek symbols

α	thermal diffusivity
δ	ratio of solidified metal layer thickness with solidification to liquid layer thickness without solidification
Λ	dimensionless term used in kinetic energy equation
ε	dimensionless positive quantity used in the estimation of initial radius
σ	surface tension
μ	viscosity
ρ	density of solid
ρ_l	density of liquid
θ	dynamic contact angle
θ_s	static contact angle
ϕ	non-dimensionalized liquid layer thickness
τ	time at which freezing begins at any radial location
ξ	non-dimensionalized radius of spreading droplet

Subscripts

max	maximum spread
0	initial condition
r	radial
z	normal

The simplicity of the Madejski model [10] and its improved version (DR model) [13] is mainly attributed to the basic assumptions made in the models. In order to formulate the initial conditions, the models assumed that the impinging spherical droplet takes the shape of cylinder immediately after the instant $t = 0$ at which the droplet touches the surface. The initial radius, R_0 was expressed as a fraction of the initial droplet diameter, D, i.e., $R_0 = \varepsilon D$, where ε is an assumed positive quantity. It must be emphasized here that the initial conditions for the droplet radius and velocity were expressed in these models [10,13] as functions of the assumed parameter ε. Madejski [10] assumed $\varepsilon = 0.5$ for the derivation of R_{max} and later, Delplanque and Rangel [13] showed that $\varepsilon = 0.74$ is the only physically possible value. However, the comparison of the model predictions with experimental results was not quite satisfactory and a better agreement was observed for $\varepsilon = 0.39$ in the early stages of impact [16]. Note that the parameter ε was treated like an arbitrary parameter in these models and any improper selection of ε may be affecting the model predictions significantly.

In the present work, we attempt to improve the predictions of the improved version of the original Madejski splat-quench solidification model (DR model) by proposing modifications for the initial conditions used to solve the governing differential equation. We keep the salient features of the original Madejski model remain intact in our modified model except that the initial conditions are derived at the instant $t_0 = \frac{D}{W}$ instead of $t_0 = 0$. The improvements noted from the present model are shown through the comparisons of present results with the corresponding predictions of DR model and experimental data.

2. Mathematical model

2.1. Droplet spreading

Consider a molten metal droplet of diameter, D impinges on a flat surface with velocity, W along the normal to the flat surface. The temperature of molten metal

droplet and flat substrate surface are, respectively, T_m and T_0. The governing differential equation for the droplet spreading process based on the conservation of mechanical energy is expressed as

$$\frac{d}{dt}(E_k + E_p + E_d) = 0 \quad (1)$$

where E_k is the kinetic energy, E_p the potential energy, E_d the viscous dissipation energy, and t, the time measured from the instant at which the droplet touches the impact surface. As in the previous studies employing Madejski's model [10,13,16,17], we assume that the impinging droplet takes the shape of cylinder with diameter, $2R$ and height, b during the spreading process. Note that earlier models implemented this assumption immediately after the instant $t = 0$. However, the experimental studies on the impact of a droplet on solid surfaces reveal that the cylindrical disc assumption may not be justifiable during the early stages of impact process [7,15,18–22]. It is shown that the droplet shape may either be a truncated sphere or a combined spherical and cylindrical disc form in the time interval showing $t^*(t^* = \frac{tW}{D})$ values ranging between 0 and 1. With D and W, respectively, as the length and velocity scales, the time at which the droplet flattens completely and forms a cylindrical disc can be expressed as $\frac{D}{W}$.

The impinging droplet spreads out radially and attains a cylindrical disc of radius, R_0 at time, $t_0 = \frac{D}{W}$ (Fig. 1(a)). By equating the total impulse of the force applied to the impact surface at $t_0 = \frac{D}{W}$ from the impinging droplet to the initial axial momentum of the droplet, Roisman et al. [23] proposed an approximate model to determine b_0, the initial thickness of the liquid layer at the instant $t_0 = \frac{D}{W}$, from the impinging droplet parameters. In their work, the simplified axial force balance equation is approximated as

$$3We + 5(1 - \cos\theta)Re\bar{b}_0 = 10ReWe\bar{b}_0^3 \quad (2)$$

The Weber number, We and Reynolds number, Re are defined, respectively, as $We = \frac{\rho_l W^2 D}{\sigma}$ and $Re = \frac{\rho_l WD}{\mu}$, where ρ_l is the density, μ, the viscosity, and σ, the surface tension of molten metal liquid. The dynamic contact angle, θ is estimated from the static contact angle, θ_s as

$$\theta = \cos^{-1}\left\{1 - 2\tanh\left[5.16\left(\frac{Ca}{1 + 1.31Ca^{0.99}}\right)^{0.706}\right]\right\} + \theta_s \quad (3)$$

where $Ca = \frac{\mu W_c}{\sigma}$ is the capillary number based on the liquid contact line velocity, W_c. Appendix A shows the details on the derivation of governing differential equation for the spreading droplet and written as

$$\frac{d}{dt}\left[\frac{3}{10}\rho_l\left(\frac{dR}{dt}\right)^2\left(R^2 b + \frac{11}{7}b^3\right) + \sigma(R^2(1 - \cos\theta) + 2Rb)\right] + \frac{\mu R^2}{b}\left(\frac{dR}{dt}\right)^2\left[\frac{3}{2} + \frac{72}{5}\frac{b^2}{R^2}\right] = 0 \quad (4)$$

Note that the governing equation used in DR model is similar to Eq. (4) except that the role of capillary forces at the contact line of the spreading droplet is ignored.

2.2. Droplet solidification

The solidification process starts immediately after the initial instant of impact ($t = 0$) and a solid metal layer starts growing over the impact surface depending on the temperature gradient from the droplet liquid to the impact surface. The thickness of the solidified metal layer, y is estimated from the Neumann solution of the one dimensional Stefan problem as

$$y = U\sqrt{\alpha t} \quad (5)$$

Here α is the thermal diffusivity of the droplet material and U, the solidification constant, expressed mathematically as a function of the Stefan number, St,

$$St = \sqrt{\pi}\left(\frac{U}{2}\right)erf\left(\frac{U}{2}\right)\exp\left(\frac{U^2}{4}\right) \quad (6)$$

where $St = \frac{C_p(T_m - T_0)}{h_f}$. C_p and h_f are the specific heat and latent heat of fusion of the droplet material, respectively.

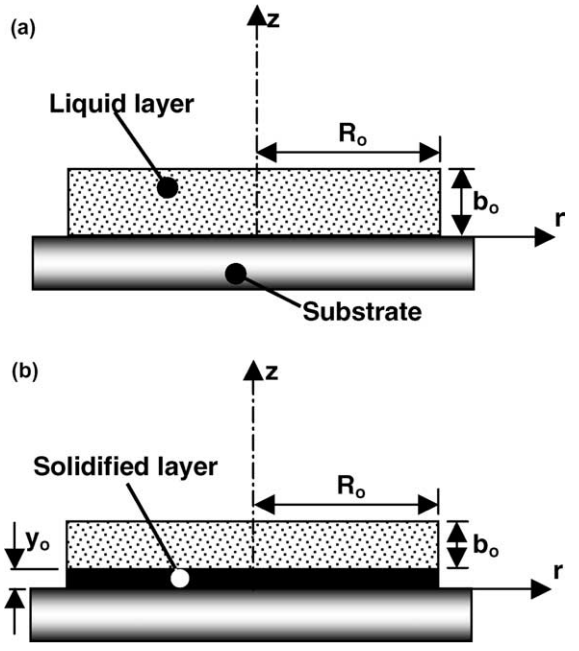

Fig. 1. The schematic illustrations showing the droplet shapes assumed in the present model at the instant $t_0 = \frac{D}{W}$. (a) Without solidification and (b) with solidification.

Note that Eqs. (5) and (6) are based on the assumption that the liquid phase is stagnant and hence, the convecting effect of the liquid phase on the solidification process is ignored in the present model.

The solidification process may be influencing the flow field in the molten liquid layer and hence the fluid pressure exerted on the impact surface. By using Eq. (5), the thickness of solidified metal layer at the instant $t_0 = \frac{D}{W}$ is estimated as

$$y\left(t_0 = \frac{D}{W}\right) = y_0 = U\sqrt{\alpha\frac{D}{W}} = \left(\frac{U}{\sqrt{Pe}}\right)D \tag{7}$$

$$\bar{y}_0 = \frac{y_0}{D} = \frac{U}{\sqrt{Pe}} \tag{8}$$

where $Pe = \frac{WD}{\alpha}$ is the Peclet number. It is assumed here in the present work that $\bar{y}_0 \ll \bar{b}_0$ and the solidification process occurring within the short interval of time $[0, \frac{D}{W}]$ during the beginning of impact process may not be altering the flow characteristics within the liquid layer significantly. Thus the effect of solidification on Eq. (2) is assumed to be negligible and consequently, the present model is more appropriate for slow solidification problems.

As the droplet is spreading along the radial direction (Fig. 2), the thickness of solidified metal layer at any radial location, r is written as

$$y(r) = U\sqrt{\alpha(t-\tau)} \tag{9}$$

where τ is the time at which freezing begins at a given r. Below, $r < R_0$ and $\tau = 0$, y is estimated from Eq. (5). The volume of the solidified metal layer, V_s is estimated as

$$V_s = \pi R_0^2 y_0 + \int_{\tau=0}^{\tau=t} 2\pi R(\tau) U\sqrt{\alpha(t-\tau)}\,\mathrm{d}R(\tau) \tag{10}$$

By including the effect of solidification, the thickness of liquid layer, b is written as

$$b = \frac{(\pi/6)D^3\rho_l - \rho V_s}{\pi R^2 \rho_l} \tag{11}$$

where ρ is the density of solidified metal layer.

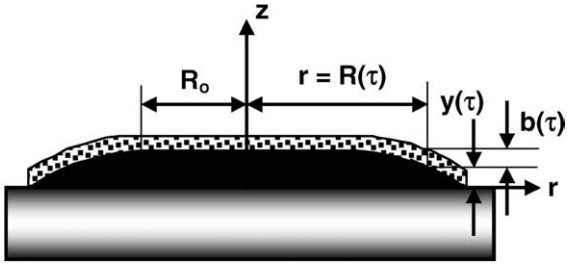

Fig. 2. The schematic sketch of the spreading droplet shape after the initial time, t_0.

2.3. Initial conditions

In the present model, the initial conditions are derived at the instant $t_0 = \frac{D}{W}$. The initial radius, R_0 is expressed in terms of $\bar{b}_0$ as

$$R\left(t_0 = \frac{D}{W}\right) = R_0 = \left(\frac{D^2}{6\bar{b}_0}\right)^{12} \tag{12}$$

The initial thickness of molten liquid layer at $t_0 = \frac{D}{W}$ is expressed by including the solidification process as

$$b\left(t_0 = \frac{D}{W}\right) = b_0 = D\left(\bar{b}_0 - \frac{U}{\sqrt{Pe}}\right) \tag{13}$$

In the absence of any solidification process, the value of U is taken as zero and b_0 is expressed only as a function of $\bar{b}_0$. The initial average radial velocity, $(\frac{\mathrm{d}R}{\mathrm{d}t})_0$ at $t_0 = \frac{D}{W}$ is derived by inserting the value of E_k calculated at $t_0 = \frac{D}{W}$ in Eq. (A.6) given in Appendix A and expressed as

$$\frac{\mathrm{d}R}{\mathrm{d}t}\left(t_0 = \frac{D}{W}\right) = \left(\frac{\mathrm{d}R}{\mathrm{d}t}\right)_0 = W\left(\frac{\frac{5}{3}\Lambda}{\left[1 - \frac{U}{\bar{b}_0\sqrt{Pe}}\right]\left[1 + \frac{66}{7}\bar{b}_0^3\left(1 - \frac{U}{\bar{b}_0\sqrt{Pe}}\right)^2\right]}\right)^{1/2} \tag{14}$$

where

$$\Lambda = 1 + \frac{12}{We} - \frac{3}{5Re}\left(\frac{1}{\bar{b}_0^3} + \frac{12}{\bar{b}_0}\right) - \frac{2(1-\cos\theta)}{We\bar{b}_0} - \frac{1}{We}\sqrt{\frac{96b_0}{D}} - \frac{U}{\bar{b}_0\sqrt{Pe}} \tag{15}$$

Further details on the derivation of Eq. (14) are given in Appendix B.

2.4. Non-dimensionalization

The energy conservation equation (Eq. (4)) and initial conditions (Eqs. (12)–(14)) are non-dimensionalized by using the variables $\xi = \frac{R}{R_0}$, $\phi = \frac{b}{R_0}$, and $\tilde{t} = \frac{Wt}{R_0}$. After simplification, Eq. (4) becomes

$$\frac{\mathrm{d}}{\mathrm{d}\tilde{t}}\left[\frac{3}{10}\left(\frac{\mathrm{d}\xi}{\mathrm{d}\tilde{t}}\right)^2\phi\left(\xi^2 + \frac{11}{7}\phi^2\right) + \frac{\sqrt{6\bar{b}_0}}{We}\xi(\xi(1-\cos\theta) + 2\phi)\right] + \frac{\sqrt{\bar{b}_0}}{Re}\frac{\xi^2}{\phi}\left(\frac{\mathrm{d}\xi}{\mathrm{d}\tilde{t}}\right)^2\left(\sqrt{\frac{27}{2}} + \frac{72\sqrt{6}}{5}\frac{\phi^2}{\xi^2}\right) = 0 \tag{16}$$

where

$$\phi = \frac{\sqrt{6}(\bar{b}_0)^{3/2}}{\xi^2}\left[1 - K\left(\sqrt{\tilde{t}} + 2\int_0^{\tilde{t}} \xi(t)\frac{\mathrm{d}\xi(t)}{\mathrm{d}t}\sqrt{(\tilde{t}-t)}\,\mathrm{d}t\right)\right] \tag{17}$$

and

$$K = \frac{\rho}{\rho_1} U \sqrt{\frac{1}{6^{1/2} Pe (\bar{b}_0)^{5/2}}} \tag{18}$$

The simplified non-dimensional initial conditions are expressed as

$$\tilde{t}\left[t_0 = \frac{D}{W}\right] = \tilde{t}_0 = \sqrt{6\bar{b}_0} \tag{19}$$

$$\xi(\tilde{t}_0) = \xi_0 = 1.0 \tag{20}$$

$$\phi(\tilde{t}_0) = \phi_0 = \sqrt{6\bar{b}_0}\left(\bar{b}_0 - \frac{U}{\sqrt{Pe}}\right) \tag{21}$$

and

$$\frac{\mathrm{d}\xi}{\mathrm{d}\tilde{t}}(\tilde{t}_0) = \left(\frac{\mathrm{d}\xi}{\mathrm{d}\tilde{t}}\right)_0 = \left(\frac{\frac{5}{3}\Lambda}{\left[1 - \frac{U}{\bar{b}_0\sqrt{Pe}}\right]\left[1 + \frac{66}{7}\bar{b}_0^3\left(1 - \frac{U}{\bar{b}_0\sqrt{Pe}}\right)^2\right]}\right)^{1/2} \tag{22}$$

3. Results and discussion

The theoretical prediction on the evolution of R is obtained by solving Eqs. (16)–(22) numerically. The predictions are made until the radial velocity of the spreading droplet reaches zero computationally. For all the calculations reported in this paper, it is ensured that the radial velocity of the spreading droplet is converging to zero. In order to show the improvements noted in the present model calculations, the present predictions are compared with the corresponding numerical predictions of DR model.

3.1. Droplet impact without solidification

The time evolution of the spreading droplet diameter ($2R$) is shown in Fig. 3 for different impact conditions. As seen in the figure, the agreement between the present model predictions and experimental data is improved both qualitatively and quantitatively. The predictions of DR model agree reasonably with the experimental data during the early stages of impact, however relies strongly on the choice of ε. In general, the modified model is slightly over predicting the values of R from the experimental data. This may be attributed to the assumptions and approximations involved in the formulation of Eqs. (2) and (14).

The comparison of results shown in Fig. 3 clearly indicates that the initial conditions used to solve the governing equation (Eq. (4)) play a major role in the predictions of the evolution of R. Fig. 4 shows the variation of non-dimensional radial velocity, $(\frac{\mathrm{d}(R/D)}{\mathrm{d}t^*})$ with time for the droplet impact case shown in Fig. 3(c). In the case of DR model predictions, the assumed parameter ε significantly influences the radial velocity during the early stages of impact as shown in Fig. 4. A noticeable change in the variation of spreading velocity is observed between the present model and DR model. The prediction of a larger droplet radius by DR model is mainly due to the higher radial velocity shown in Fig. 4. Thus the improvements noted in the present model predictions of R are attributed to the initial radial velocity relation given in Eq. (14).

The present model predictions on the maximum droplet radius, $R_{\max}$ reached during the impact process is shown in Fig. 5 for different droplet impact experiments reported in the literature. A total of 33 experiments with different impact conditions are considered for the comparison. As mentioned earlier, the present model is over predicting $R_{\max}$ with a variation of 20% from the experimental values. Fig. 6 shows the model predictions on the non-dimensional time parameter, $(\frac{tW}{D})_{\max,0.95}$, at which the spreading droplet radius reaches $0.95R_{\max}$ for different droplet impact experiments. The predicted values of $(\frac{tW}{D})_{\max,0.95}$ are more distributed around the 45° line compared to the predictions of $R_{\max}$ shown in Fig. 5.

3.2. Droplet impact with solidification

The primary cause for the spreading droplet solidification is the temperature gradient exists between the droplet liquid and the impact surface. Therefore the effect of solidification can be seen from the variation of St. For instance, a rapid solidification of the spreading droplet liquid can be observed for the droplet impact with high St. Fig. 7 shows the time evolution of R predicted by the present model for the molten tin droplets impinging on the stainless steel surfaces kept at high temperatures and hence low St cases. As done for the droplet impact cases without solidification, the results are presented in Fig. 7 along with the predictions of DR model and experimental data. In general, the predictions of R obtained from the present model calculations are in good agreement with the experimental data, both qualitatively and quantitatively, and the predictions of DR model are far deviated from the experimental data. The model predictions of $R_{\max}$ for different cases of molten metal droplet impact are shown in Fig. 8. A good

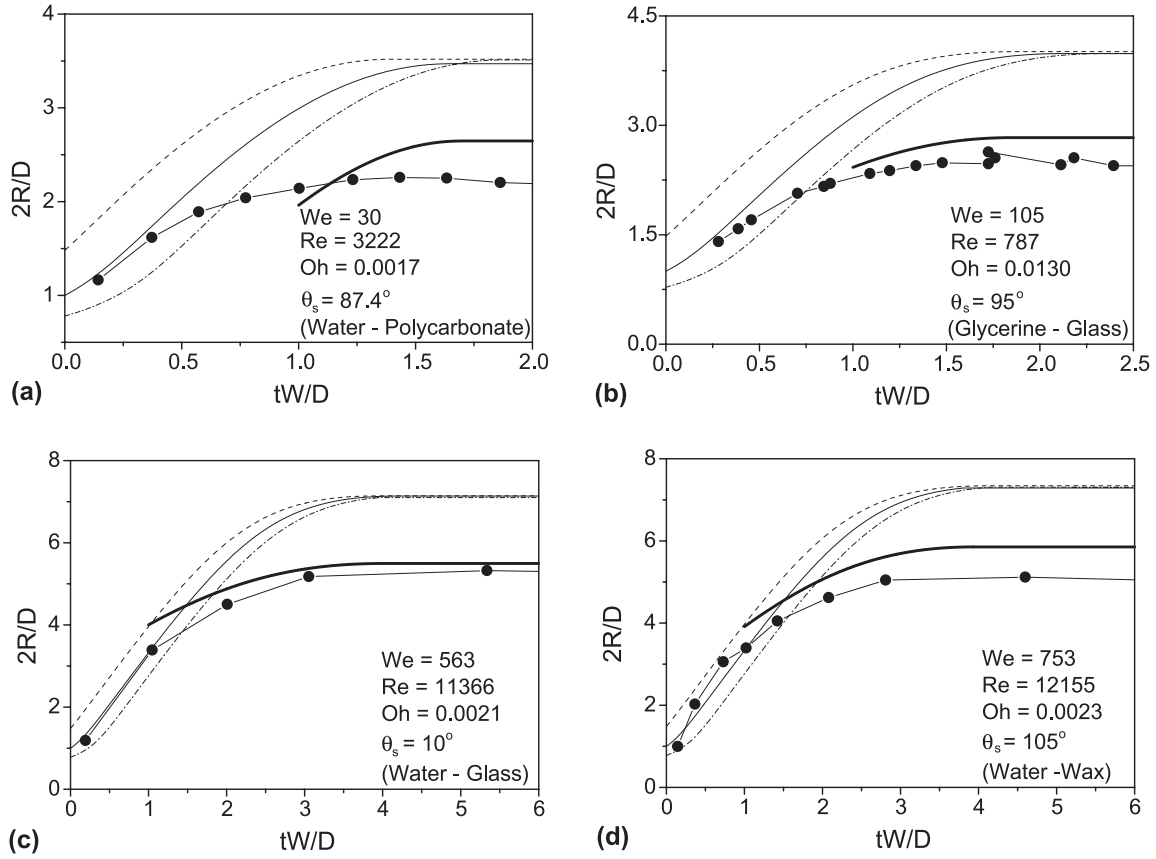

Fig. 3. Comparison of the present model results on the evolution of the spreading liquid droplets with the predictions of DR model and experimental data. The experimental data are shown with filled circles (●) and the numerical predictions obtained from the present model are shown with a thick continuous line (—). The predictions of DR model for different values of ε are shown with thin lines: (– – –) $\varepsilon = 0.74$, (——) $\varepsilon = 0.5$, (–·–·–) $\varepsilon = 0.39$. The experimental data are taken from the literature. (a) Kim and Chun [21], (b) Roisman et al. [23], (c) Rioboo et al. [22], and (d) Roisman et al. [23].

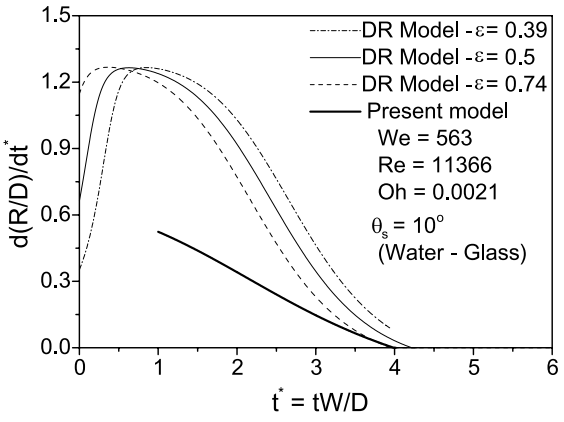

Fig. 4. Comparison of the present model results on the variation of non-dimensional radial velocity with the predictions of DR model for the droplet impact case shown in Fig. 3(c).

agreement is observed between the experimental data and present model predictions particularly for the droplet impact with high *We*. Note that the present calculation is ignored the heat transfer processes exist between the spreading droplet liquid and the substrate. Since the temperature gradient for the droplet impact cases shown in Figs. 7 and 8 is small, the above assumption may not be expected to alter the conclusions arrived from this study.

3.3. Discussion

It is shown in the previous sections that the present model, based on the splat-quench solidification model proposed by Madejski [10], predicts the spreading and solidification processes of the molten metal droplets impinging on the solid surfaces quite well compared to the earlier version, DR model [13]. The theoretical predictions obtained from the previous studies based on the

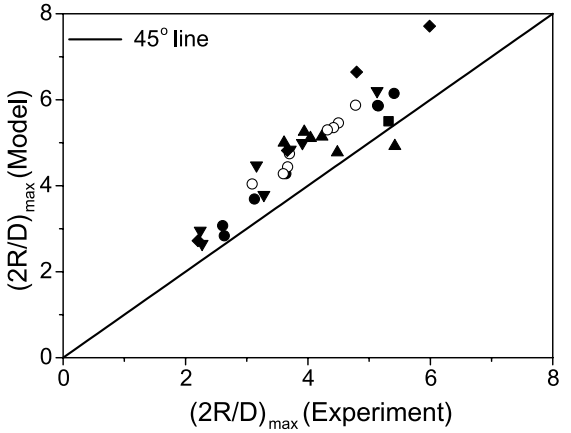

Fig. 5. The present model predictions on the maximum droplet radius, R_{max} for the droplet impact experiments reported in earlier work. (●) Roisman et al. [23], (■) Rioboo et al. [22], (▲) Fukai et al. [19], (▼) Kim and Chun [21], (◆) Aziz and Chandra [15], and (○) Mao et al. [20].

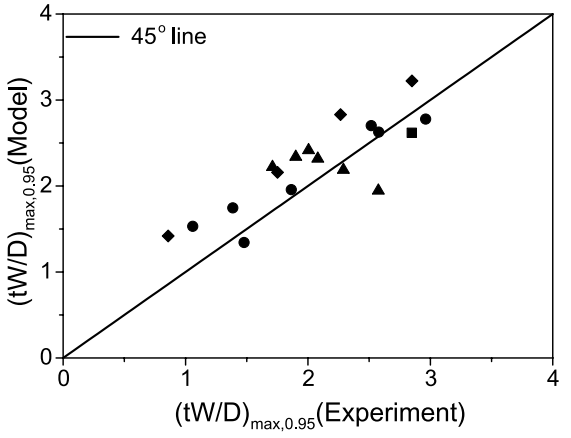

Fig. 6. The present model predictions of $(\frac{tW}{D})_{max,0.95}$ for the droplet impact experiments reported in earlier work. (●) Roisman et al. [23], (■) Rioboo et al. [22], (▲) Fukai et al. [19], and (◆) Aziz and Chandra [15].

original Madejski model [13,14,17] are predominantly depending on the choice of ε and this constraint is removed in the present modified model as the initial conditions are directly obtained from the impinging droplet parameters. The major limitation of the present model is that it ignores the calculations within the time interval $[0, \frac{D}{W}]$. This restricts the model applications for the droplet impact problems involving rapid solidification process.

Although the present predictions of R_{max} obtained for the impact of molten solder metal droplets [26] are comparable with the experimental measurements (indicated by open circles in Fig. 8) the present model may not be suitable for such droplet impact cases. At low *We*, the droplet spreading process is influenced significantly by the capillary forces and hence, the solidification process may be either competing with or dominating the spreading process. This may be resulting in a complete solidification of the spreading droplet liquid before reaching the instant $t_0 = \frac{D}{W}$. Note that the droplet impact cases shown in Fig. 7 are in the regime of high impact *We* and *Re*. Under these conditions, the radial spreading is dominating the solidification process due to high fluid inertia and hence, the approximations involved in Eq. (14) may not be influencing the predictions significantly.

For the droplet impacts involving rapid solidification process, the majority of molten metal liquid solidifies before reaching the instant $\frac{tW}{D} = 1$. A non-dimensional parameter, δ is defined as the ratio of the solidified metal layer height to the metal liquid layer height in the absence of solidification. At $t_0 = \frac{D}{W}$, δ is expressed as

$$\delta_0 = \frac{y_0}{\bar{b}_0 D} = \frac{1}{\bar{b}_0}\frac{U}{\sqrt{Pe}} \tag{23}$$

The present model is applicable for the molten droplet impact cases with $\delta_0 \to [0,1)$. From Eq. (6), U can be approximated in terms of St by employing curve fitting technique as $U \approx \sqrt{\frac{5St}{3}}$, and hence

$$\delta_0 \approx \frac{1}{\bar{b}_0}\sqrt{\frac{5St}{3Pe}} \tag{24}$$

By following Eq. (24), it can be stated that the present model is more suitable for the molten droplet impact cases with a lower value of $\frac{St}{Pe}$ and a higher value of $\bar{b}_0$. The values of $\frac{St}{Pe}$ for the molten solder droplet impact cases shown in Fig. 8 (indicated by open circles) are in the range 2.84×10^{-2} to 8.09×10^{-2}, which is one order of magnitude higher than the cases shown in Fig. 7(a) ($\frac{St}{Pe} = 1.7\times10^{-3}$) and 7(b) ($\frac{St}{Pe} = 8.0\times10^{-4}$).

4. Conclusions

The impact behavior of the molten metal droplets is studied theoretically by formulating a model based on the improved version of the original Madejski's splat-quench solidification model. The salient features of the present model are mainly confined to the initial conditions proposed to solve the governing energy equation. The new initial conditions are modeled at time $t_0 = \frac{D}{W}$ from the start of impact. The numerical predictions on the evolution of the spreading droplet radius are obtained for different droplet impact cases and compared with the experimental data reported in the literature. The qualitative and quantitative agreements between the current predictions and experimental data are good. It is shown from qualitative arguments that the current model is more suitable for the impact problems of molten metal droplets involving slow solidification process.

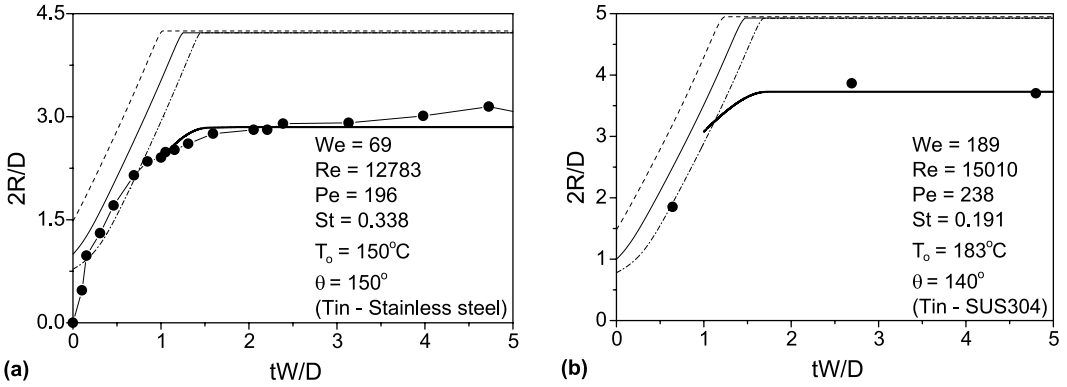

Fig. 7. Comparison of the present model results on the evolution of the spreading molten tin droplets with the predictions of DR model and experimental data. The legends are as shown in the caption of Fig. 3. The experimental data are taken from the literature. (a) Pasandideh-Fard et al. [8], and (b) Yang et al. [25].

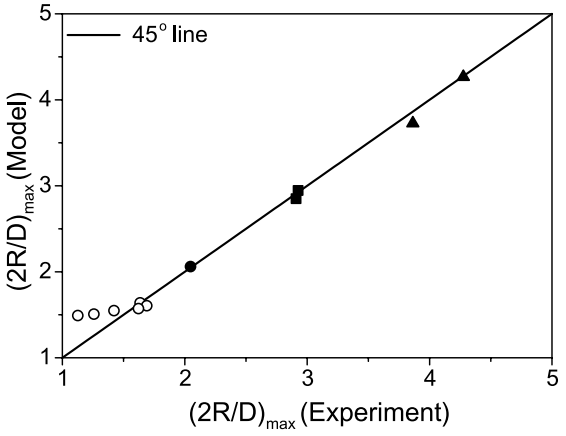

Fig. 8. The present model predictions on the maximum droplet radius, R_{max} for the molten metal droplet impact experiments reported in earlier work. (●) Aziz and Chandra [15], (■) Pasandideh-Fard et al. [8], (▲) Yang [25], and (○) Attinger et al. [26].

Acknowledgements

This research has been supported by Japan Society for the Promotion of Science (JSPS) during 2003–2004. Previous stay of D.S. at Technical University of Darmstadt, Germany is gratefully acknowledged.

Appendix A. The governing differential equation for the droplet spreading process

The governing differential equation for the droplet deformation process based on the conservation of mechanical energy is expressed as

$$\frac{\mathrm{d}}{\mathrm{d}t}(E_\mathrm{k} + E_\mathrm{p} + E_\mathrm{d}) = 0 \tag{A.1}$$

The expressions for the energy terms E_k and E_d shown in Eq. (A.1) can be obtained from the similar procedure followed in DR model [13]. The flow field in the spreading liquid layer is described by [24]

$$W_\mathrm{z} = 2C\left(\frac{z^3}{3} - bz^2\right) \tag{A.2}$$

and

$$W_\mathrm{r} = Cr(2zb - z^2) \tag{A.3}$$

where C is a time dependent quantity and expressed in terms of $\frac{\mathrm{d}R}{\mathrm{d}t}$, the average radial velocity on the periphery of the spreading droplet, as

$$C = \frac{3}{2Rb^2}\frac{\mathrm{d}R}{\mathrm{d}t} \tag{A.4}$$

The kinetic energy term E_k is evaluated from

$$E_\mathrm{k} = \pi\int_0^R r\,\mathrm{d}r\int_0^b \rho_\mathrm{l}(W_x^2 + W_\mathrm{r}^2)\,\mathrm{d}z \tag{A.5}$$

By substituting Eqs. (A.2) and (A.3) in Eq. (A.5), E_k is expressed as

$$E_\mathrm{k} = \frac{3}{10}\pi\rho_\mathrm{l}\left(\frac{\mathrm{d}R}{\mathrm{d}t}\right)^2\left(R^2b + \frac{11}{7}b^3\right) \tag{A.6}$$

The rate of viscous dissipation, $\frac{\mathrm{d}E_\mathrm{d}}{\mathrm{d}t}$ is evaluated from

$$\frac{\mathrm{d}E_\mathrm{d}}{\mathrm{d}t} = \int_V \Phi\,\mathrm{d}V \tag{A.7}$$

where

$$\Phi = \mu\left[2\left(\frac{\partial W_\mathrm{r}}{\partial r}\right)^2 + 2\frac{W_\mathrm{r}^2}{r^2} + 2\left(\frac{\partial W_\mathrm{z}}{\partial z}\right)^2 + \left(\frac{\partial W_\mathrm{r}}{\partial r}\right)^2\right] \tag{A.8}$$

By using Eqs. (A.2), (A.3), (A.7) and (A.8),

$$\frac{dE_d}{dt} = \frac{\pi\mu R^2}{b}\left(\frac{dR}{dt}\right)^2\left(\frac{3}{2}+\frac{72}{5}\frac{b^2}{R^2}\right) \tag{A.9}$$

The estimation of E_p proposed in DR model is not included the effect of capillary forces at the contact line of the spreading droplet. Though the role of capillary forces is less significant during the initial spreading regime, it becomes more important towards the maximum spreading regime at which the inertial forces become comparable or small. By including the capillary forces at the contact line, E_p is expressed as

$$E_p = \sigma\pi R^2(1-\cos\theta) + \sigma 2\pi R b \tag{A.10}$$

By using Eqs. (A6), (A.9) and (A.10), the equation for the droplet spreading process, Eq. (A.1) can be written as

$$\frac{d}{dt}\left[\frac{3}{10}\rho_l\left(\frac{dR}{dt}\right)^2\left(R^2 b+\frac{11}{7}b^3\right)+\sigma(R^2(1-\cos\theta)+2Rb)\right] + \frac{\mu R^2}{b}\left(\frac{dR}{dt}\right)^2\left[\frac{3}{2}+\frac{72}{5}\frac{b^2}{R^2}\right] = 0 \tag{A.11}$$

Appendix B. The derivation for the initial radial velocity

The principle of energy conservation at the instant $t_0 = \frac{D}{W}$ is written as

$$\left\{[\mathrm{KE}+\mathrm{PE}]_{\mathrm{liquid}} + [\mathrm{Energy\ due\ to\ wetting}] + [\mathrm{KE}+\mathrm{Viscous\ dissipation}]_{\mathrm{losses}}\right\}_{t_0=\frac{D}{W}} = \{[\mathrm{KE}+\mathrm{PE}]_{\mathrm{liquid}}\}_{t=0}.$$

The initial kinetic and potential energies of the impinging droplet are estimated as

$$\{(\mathrm{KE})_{\mathrm{liquid}}\}_{t=0} = \left(\frac{\pi D^3}{6}\right)\left(\frac{1}{2}\rho_l W^2\right) \tag{B.1}$$

and

$$\{(\mathrm{PE})_{\mathrm{liquid}}\}_{t=0} = \sigma(\pi D^2) \tag{B.2}$$

At the instant $t_0 = \frac{D}{W}$, it is expressed that

$$\{[\mathrm{KE}]_{\mathrm{liquid}}\}_{t_0=\frac{D}{W}} = E_k\left(t_0 = \frac{D}{W}\right) \tag{B.3}$$

$$\{[\mathrm{PE}]_{\mathrm{liquid}}\}_{t_0=\frac{D}{W}} = \sigma(\pi R_0^2 + 2\pi R_0 b_0) \tag{B.4}$$

and

$$\{[\mathrm{KE}]_{\mathrm{losses}}\}_{t_0=\frac{D}{W}} = (\pi R_0^2 y_0)\left(\frac{1}{2}\rho_l W^2\right) = \pi\rho_l W^2 D^3\left(\frac{U}{12\bar{b}_0\sqrt{Pe}}\right) \tag{B.5}$$

The total viscous dissipation losses at $t_0 = \frac{D}{W}$ is calculated from

$$\{[\mathrm{Viscous\ dissipation}]_{\mathrm{losses}}\}_{t_0=\frac{D}{W}} = \int_0^{D/W}\int_0^{R_0}\int_0^{b_0} 2\pi r\Phi\,dr \tag{B.6}$$

Since the present model ignores the effect of solidification process on the molten metal liquid layer during the time interval $[0, \frac{D}{W}]$, no attempt is made in the present work to modify the viscous dissipation losses for the solidification process. Note that the flow field of the spreading droplet described in the present work is similar to the flow field used by Roisman et al. [23] and hence, by following the procedure adopted by Roisman et al. [23], the viscous dissipation is expressed as

$$\{[\mathrm{Viscous\ dissipation}]_{\mathrm{losses}}\}_{t_0=\frac{D}{W}} = \pi\rho_l D^3 W^2\frac{1}{Re}\left(\frac{1}{20\bar{b}_0^3}+\frac{3}{5\bar{b}_0}\right) \tag{B.7}$$

The energy due to wetting is written as

$$[\mathrm{Energy\ due\ to\ wetting}]_{t_0=\frac{D}{W}} = \sigma(\pi R_0^2\cos\theta) \tag{B.8}$$

By substituting Eqs. (B.1)–(B.8) in the energy conservation relation, the kinetic energy of the spreading droplet at $t_0 = \frac{D}{W}$ is expressed as

$$E_k\left(t=\frac{D}{W}\right) = E_{k0} = \Lambda(\bar{b}_0, Re, We, \theta)\left(\frac{\pi\rho_l D^3 W^2}{12}\right) \tag{B.9}$$

where

$$\Lambda = 1+\frac{12}{We}-\frac{3}{5Re}\left(\frac{1}{\bar{b}_0^3}+\frac{12}{\bar{b}_0}\right)-\frac{2(1-\cos\theta)}{We\bar{b}_0} - \frac{1}{We}\sqrt{\frac{96b_0}{D}}-\frac{U}{\bar{b}_0\sqrt{Pe}} \tag{B.10}$$

By comparing Eq. (B.10) with Eq. (A.6) shown in Appendix A, the initial spreading velocity is obtained as

$$\frac{dR}{dt}\left(t=\frac{D}{W}\right) = \left(\frac{dR}{dt}\right)_0 = W\left(\frac{\frac{5}{3}\Lambda}{\left[1-\frac{U}{\bar{b}_0\sqrt{Pe}}\right]\left[1+\frac{66}{7}\bar{b}_0^3\left(1-\frac{U}{\bar{b}_0\sqrt{Pe}}\right)^2\right]}\right)^{1/2} \tag{B.11}$$

References

[1] L. Pawlowski, The Science and Engineering of Thermal Spray Coatings, Wiley, New York, 1995.
[2] F. Gao, A.A. Sonin, Precise deposition of molten microdrops: the physics of digital microfabrication, Proc. Royal Soc. A 444 (1994) 533–554.

[3] E.J. Lavernia, Y. Wu, Spray Atomization and Deposition, John Wiley and Sons, UK, 1996.
[4] L.J. Zarzalejo, K.S. Schmaltz, C.H. Amon, Molten droplet solidification and substrate remelting in microcasting. Part I: numerical modeling and experimental verification, Heat Mass Transfer 34 (1999) 477–485.
[5] Q. Liu, M. Orme, High precision solder droplet printing technology and the state-of-the-art, J. Mater. Process. Tech. 115 (2001) 272–283.
[6] Z. Zhao, D. Poulikakos, J. Fukai, Heat transfer and fluid dynamics during the collision of a liquid droplet on a substrate—I. Modeling, Int. J. Heat Mass Transfer 39 (1996) 2771–2789.
[7] Z. Zhao, D. Poulikakos, J. Fukai, Heat transfer and fluid dynamics during the collision of a liquid droplet on a substrate—II. Experiments, Int. J. Heat Mass Transfer 39 (1996) 2791–2809.
[8] M. Pasandideh-Fard, R. Bhola, S. Chandra, J. Mostaghimi, Deposition of tin droplets on a steel plate: simulations and experiments, Int. J. Heat Mass Transfer 41 (1998) 2929–2945.
[9] H. Jones, Cooling, freezing and substrate impact of droplets formed by rotary atomization, J. Phys. D: Appl. Phys. 4 (1971) 1657–1660.
[10] J. Madejski, Solidification of droplets on a cold surface, Int. J. Heat Mass Transfer 19 (1976) 1009–1013.
[11] G. Trapage, E.F. Matthys, J.J. Valencia, J. Szekely, Fluid flow, heat transfer, and solidification of molten metal droplets impinging on substrates: comparison of numerical and experimental results, Metall. Trans. 23B (1992) 701–718.
[12] T. Bennet, D. Poulikakos, Splat-quench solidification: estimating the maximum spreading of a droplet impacting on a solid surface, J. Mater. Sci. 28 (1993) 963–970.
[13] J.-P. Delplanque, R.H. Rangel, An improved model for droplet solidification on a flat surface, J. Mater. Sci. 32 (1997) 1519–1530.
[14] H. Zhang, Theoretical analysis of spreading and solidification of molten droplet during thermal spray deposition, Int. J. Heat Mass Transfer 42 (1999) 2499–2508.
[15] S.D. Aziz, S. Chandra, Impact, recoil and splashing of molten metal droplets, Int. J. Heat Mass Transfer 43 (2000) 2841–2857.
[16] J.-P. Delplanque, R.H. Rangel, A comparison of models, numerical simulation, and experimental results in droplet deposition processes, Acta Mater. 46 (1998) 4925–4933.
[17] Y.P. Wan, H. Zhang, X.Y. Jiang, S. Sampath, V. Prasad, Role of solidification, substrate temperature and Reynolds number on droplet spreading in thermal spray deposition: measurements and modeling, ASME J. Heat Transfer 123 (2001) 382–389.
[18] S. Chandra, C.T. Avedisian, On the collision of a droplet with a solid surface, Proc. R. Soc. Lond. A 432 (1991) 13–41.
[19] J. Fukai, Y. Shiba, T. Yamamoto, O. Miyatake, D. Poulikakos, C.M. Megaridis, Z. Zhao, Wetting effects on the spreading of a liquid droplet colliding with a flat surface: experimental and modeling, Phys. Fluids 7 (1995) 236–247.
[20] T. Mao, D.C.S. Kuhn, H. Tran, Spread and rebound of liquid droplets upon impact on flat surfaces, AIChE J. 43 (1997) 2169–2179.
[21] H.-Y. Kim, J.-H. Chun, The recoiling of liquid droplets upon collision with solid surfaces, Phys. Fluids 13 (2001) 643–659.
[22] R. Rioboo, M. Marengo, C. Tropea, Time evolution of liquid drop impact onto solid, dry surfaces, Exp. Fluids 33 (2002) 112–124.
[23] I.V. Roisman, R. Rioboo, C. Tropea, Normal impact of a liquid drop on a dry surface: model for spreading and receding, Proc. R. Soc. Lond. A 458 (2002) 1411–1430.
[24] A.J. Markworth, J.H. Saunders, An improved velocity field for the Madejski splat-quench solidification model, Int. J. Heat Mass Transfer 35 (1992) 1836–1837.
[25] Y.-S. Yang, H.-Y. Kim, J.-H. Chun, Spreading and solidification of a molten microdrop in the solder jet pumping process, IEEE Trans. Compon. Packag. Technol. 26 (2003) 215–221.
[26] D. Attinger, Z. Zhao, D. Poulikakos, An experimental study of molten microdroplet surface deposition and solidification: transient behavior and wetting angle dynamics, ASME J. Heat Transfer 122 (2000) 544–555.